

# Detonation spraying of TiO<sub>2</sub>–2.5 vol.% Ag powders in a reducing atmosphere

Dina V. Dudina<sup>a,\*</sup>, Sergey B. Zlobin<sup>b</sup>, Natalia V. Bulina<sup>a</sup>, Alexey L. Bychkov<sup>a</sup>,  
Vladimir N. Korolyuk<sup>c</sup>, Vladimir Yu. Ulianitsky<sup>b</sup>, Oleg I. Lomovsky<sup>a</sup>

<sup>a</sup> Institute of Solid State Chemistry and Mechanochemistry SB RAS, Kutateladze str. 18, Novosibirsk 630128, Russia

<sup>b</sup> Lavrentiev Institute of Hydrodynamics SB RAS, Lavrentiev Ave. 15, Novosibirsk 630090, Russia

<sup>c</sup> Institute of Geology and Mineralogy, Koptug Ave. 3, Novosibirsk 630090, Russia

Received 15 August 2011; received in revised form 4 October 2011; accepted 16 October 2011

Available online 10 November 2011

## Abstract

In the present work, rutile powders containing additions of metallic silver (2.5 vol.%) were detonation sprayed in a reducing atmosphere formed by gaseous detonation products of the C<sub>2</sub>H<sub>2</sub> + 1.05O<sub>2</sub> mixture. The initial volume of the C<sub>2</sub>H<sub>2</sub> + 1.05O<sub>2</sub> mixture – explosive charge – used for a detonation pulse was computer-controlled as the fraction of the barrel volume filled with the mixture. Using a previously developed model of the detonation process, the particle temperatures and velocities were calculated to explain the observed phase and microstructure development in the coatings. With increasing explosive charge, the temperature of the sprayed particles increased and rutile was partially reduced to oxygen-deficient TiO<sub>2-x</sub> and then to Ti<sub>3</sub>O<sub>5</sub>. When the melting temperature of rutile was not reached, the coatings were porous; semi-molten particles formed denser coatings obtained with higher spraying efficiency. Silver inclusions in the titanium oxide matrix experienced melting and substantial overheating, but remained well preserved in the coatings.

© 2011 Elsevier Ltd. All rights reserved.

**Keywords:** TiO<sub>2</sub>; Detonation spraying; Electron microscopy; Microstructure

## 1. Introduction

Possibilities of controlling the composition and microstructure of thermally sprayed coatings by variation of spraying parameters attract attention of many researchers and coating manufacturing engineers.<sup>1–4</sup> For ceramic materials, partial or complete melting of the sprayed particles is necessary to provide high spraying efficiency and form coatings of good cohesion between the layers in a deposit and good adhesion to the substrate. It is rather common for thermal spraying to deal with issues of oxidation of sensitive materials and the presence of undesirable oxide phases reducing the quality of the substrate/coating interface and influencing the properties of the coatings. In this work, we show that it is possible to benefit from the use of high temperatures if the spraying is conducted under

a reducing atmosphere, and, instead of oxidation, a controlled reduction process can be implemented.

The subject of this study is TiO<sub>2</sub>–2.5 vol.% Ag coatings deposited on copper substrates from composite powders prepared by solid-state mixing of titanium dioxide (rutile) and elemental silver. Titanium dioxide has become the subject of numerous investigations owing to its exciting properties, such as photocatalytic activity<sup>5,6</sup> and biocompatibility.<sup>7</sup> Upon losing oxygen, titanium dioxide becomes catalytically active due to formation of crystallographic shear structures<sup>8</sup> and works as a photocatalyst in visible light.<sup>9,10</sup> Addition of metallic silver particles to TiO<sub>2</sub> improves its photocatalytic behavior<sup>11</sup> and imparts antibacterial properties to the composite material.<sup>12–14</sup> In most applications, it is the surfaces of materials that should exhibit antibacterial activity. TiO<sub>2</sub>–Ag coatings may protect copper coils of air-conditioners preventing accumulation and growth of bacteria on the coil surfaces.

The choice of the deposition technique for the TiO<sub>2</sub>–Ag coatings is dictated by a lack of inherent plasticity in titanium dioxide making it necessary to use thermal spraying as opposed

\* Corresponding author. Tel.: +7 383 316 58 42; fax: +7 383 332 28 47.  
E-mail address: [dina1807@gmail.com](mailto:dina1807@gmail.com) (D.V. Dudina).

to cold spraying to efficiently deposit  $\text{TiO}_2$  layers well-bonded to substrates. Most commonly,  $\text{TiO}_2$ -based coatings are produced by plasma spraying and high-velocity oxy-fuel (HVOF) spraying.<sup>13,15–21</sup> The appearance of anatase in the coatings sprayed from rutile powders has been previously addressed<sup>17,20</sup> and related to rapid cooling of the deposits upon impact. Reduction of  $\text{TiO}_2$  during plasma spraying has been reported, however, no parameter has been proposed to control the content of sub-oxides or oxygen-deficient rutile in the coating.<sup>16,18,20</sup>

Recent developments in the detonation spraying make it attractive for producing dense coatings of good adhesion.<sup>1,4</sup> In detonation spraying, the powder particles are fed into the barrel of a detonation gun filled with an explosive gaseous mixture. With the development of computer-controlled detonation spraying,<sup>4</sup> it has become possible to precisely control the amount of an explosive gaseous mixture in the detonation gun as well as its chemical composition. In this work, we demonstrate that during detonation spraying of rutile in a reducing atmosphere, the phase composition of the coatings can be controlled by the amount of an explosive gaseous mixture. In order to rationalize the observed phase changes and microstructure formation of the coatings, we involve calculations of temperatures and velocities of the sprayed particles.

## 2. Materials and methods

Titanium dioxide (rutile, 99.999% purity, average particle size 30  $\mu\text{m}$ ) and silver (99.99% purity, average particle size 0.5  $\mu\text{m}$ ) powders were used to prepare the powders mixtures for the detonation spraying. The mixtures corresponding to the  $\text{TiO}_2$ –2.5 vol.% Ag composition were ball milled in a high energy ball mill (AGO-type<sup>22</sup>) using a ball acceleration of 200  $\text{m s}^{-2}$ . The time of treatment was 5 min, the ball to powder ratio was 20/1. Stainless steel vials and balls were used. The purpose of ball milling was to form a composite structure in the powders with a uniform distribution of Ag particles. The highest efficiency of deposition in the detonation spraying is achieved when the sprayed particles are several tens of microns in size.<sup>1</sup> As will be shown below, the milled  $\text{TiO}_2$ –2.5 vol.% Ag powders contained a large fraction of very fine particles (less than 5  $\mu\text{m}$  in size) unsuitable for detonation spraying. A procedure was developed to agglomerate the milled powders, which included mixing the powders with a 10 wt.% polyvinyl alcohol (PVA) water solution (the weight ratio of the PVA solution to the powders was 3:7), drying the paste and sieving the dry product through a 71  $\mu\text{m}$  sieve.

A computer controlled detonation spraying (CCDS) facility<sup>4</sup> was used to deposit the coatings. The barrel of the detonation gun was 850 mm long and 20 mm in diameter. Acetylene  $\text{C}_2\text{H}_2$  was used as a fuel. The composition of the explosive mixture was  $\text{C}_2\text{H}_2 + 1.05\text{O}_2$ , which provided a reducing environment for the sprayed particles due to the presence of hydrogen and carbon monoxide in the detonation products.<sup>4</sup> The fraction of the volume of the gun barrel filled with the explosive mixture was varied in the range of 30–60%. The powder injection point was located 350 mm from the open end of the barrel. The injection was performed by a powder feeder. The spraying distance

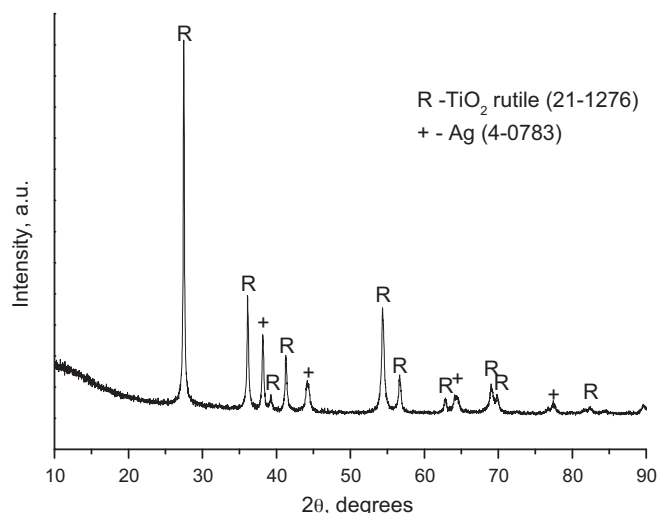


Fig. 1. XRD pattern of the  $\text{TiO}_2$ –2.5 vol.% Ag powders used for detonation spraying.

was set at 150 mm. The coatings were deposited on copper substrates 1 mm thick. The substrates were sand-blasted before the deposition of coatings. The weight of the substrates before and after the deposition was accurately measured. The samples of coatings were produced with 20 shots of the detonation gun.

The detonation gun used in this work produces a coating on a substrate with the following geometrical features: the deposit consists of a central spot about 20 mm in diameter and a peripheral area of reduced thickness of the coating. The coating has a uniform microstructure across the central spot. This central area was used to characterize the coatings. The microstructure of the coatings was studied by Scanning Electron Microscopy (SEM) and Energy Dispersive Spectroscopy (EDS) using a Hitachi-Tabletop TM-1000 Scanning Electron Microscope with a back-scattered electron detector. The XRD phase analysis of the coatings was performed using an X-ray diffractometer (D8 ADVANCE, Bruker) with  $\text{Cu K}\alpha$  radiation.

In order to estimate the velocities and temperatures of the particles at the exit point of the detonation gun, a previously developed numerical model was used.<sup>23</sup> This model has been recently validated both for particle velocity<sup>24</sup> and temperature upon collision with a substrate<sup>25</sup>. The calculations were performed using the thermodynamic data for rutile<sup>26–28</sup> and silver.<sup>27</sup>

## 3. Results and discussion

XRD pattern of the milled  $\text{TiO}_2$ –2.5 vol.% Ag powder (Fig. 1) confirms its two-phase structure. A large fraction of micron and submicron sized particles in the mechanically milled powders (Fig. 2a) made them unsuitable for a direct use in the detonation spraying. In order to produce agglomerates 10–60  $\mu\text{m}$  in size, the powders were agglomerated with a PVA-binder. The morphology of the agglomerated  $\text{TiO}_2$ –2.5 vol.% Ag powders is shown in Fig. 2b. The powder agglomerates were strong enough to provide sufficient flowability of the powders, which is essential for efficient injection of the powder into the gun barrel with a feeder.

Table 1

Calculated temperatures ( $T$ ) and velocities ( $V$ ) of the  $\text{TiO}_2$ –2.5 vol.% Ag particles exiting the barrel of the detonation gun. The calculations were performed for particles 20, 40 and 60  $\mu\text{m}$  in diameter and the distance traveled by the particles in the gun barrel equal to 350 mm.

Volume fraction of the barrel filled with $1.05\text{O}_2 + \text{C}_2\text{H}_2$ mixture, %	20 $\mu\text{m}$		40 $\mu\text{m}$		60 $\mu\text{m}$	
	$V, \text{m s}^{-1}$	$T, \text{K}$	$V, \text{m s}^{-1}$	$T, \text{K}$	$V, \text{m s}^{-1}$	$T, \text{K}$
30	550	780	430	1320	360	1120
40	610	1600	510	1700	430	1400
50	690	2120	560	1980	460	1640
60	680	2650	530	2120	420	2040

The calculated temperatures and velocities of the  $\text{TiO}_2$ –2.5 vol.% Ag particles exiting the barrel of the detonation gun are presented in Table 1. As the explosive charge increases, the sprayed particles experience more intensive heating. The calculations were performed for 20, 40 and 60  $\mu\text{m}$  particles showing that the particle temperature depended on their size. When the explosive charge is 50–60% of the gun barrel volume, smaller particles are heated up to a higher extent than larger particles, while at smaller explosive charges of 30–40%, the hottest particles are those of 40  $\mu\text{m}$  in size. The melting temperature of rutile (2123 K) was not reached at an

explosive charge of 30%. As was calculated for the average distance traveled by the particles of 350 mm, the particle temperatures did not reach the melting point of rutile at an explosive charge of 40%, either. However, according to the model used for the calculations, the difference in the location of the starting point can be a source of significant deviations in the particle temperature. While the average distance traveled by the powder particles in the detonation gun was 350 mm, some particles could start their travel 300 mm or 400 mm from the open end of the barrel. The temperature difference can be several hundred degrees and is greater for smaller particles and higher-temperature conditions. Despite this uncertainty in the particle temperature, the calculations help rationalize the observed microstructures and determine the role of the molten phases during deposition. So, if some 20  $\mu\text{m}$ -sized particles start their travel in the gun barrel 400 mm from its open end, they partially melt.

The calculated particle velocities increase as the explosive charge increases from 30 to 50%; at 60% there is a slight drop in the particle velocity. This non-monotonous dependence of the particle velocity on the explosive charge has been previously elucidated<sup>4</sup> and is related to the relative position of the powder injection point and the end of the barrel volume filled with the explosive mixture.

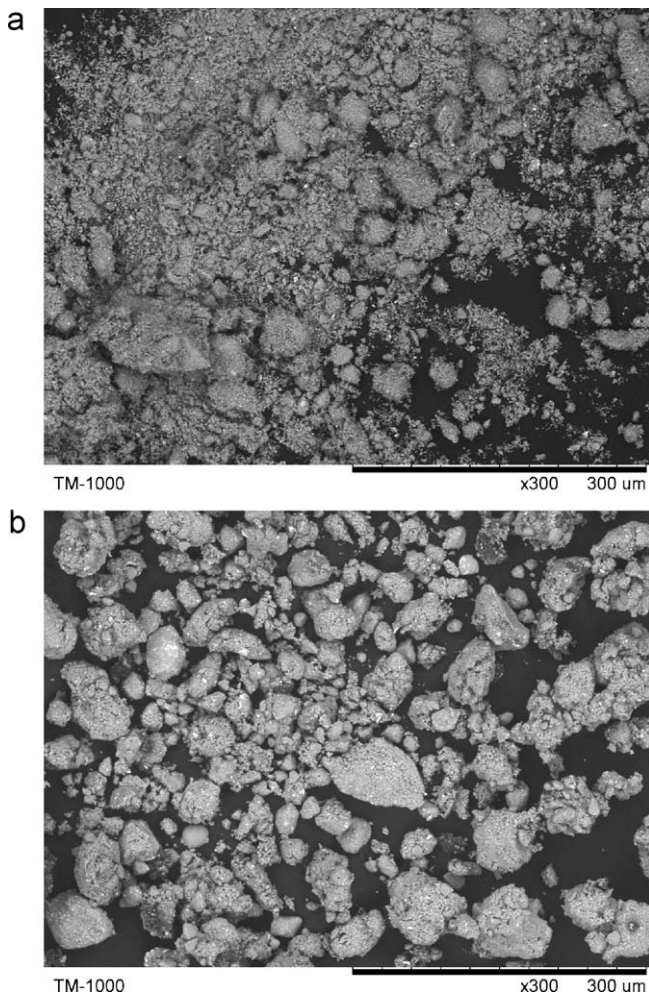


Fig. 2. SEM images of the  $\text{TiO}_2$ –2.5 vol.% Ag powders: (a) as-milled, (b) agglomerated with PVA.

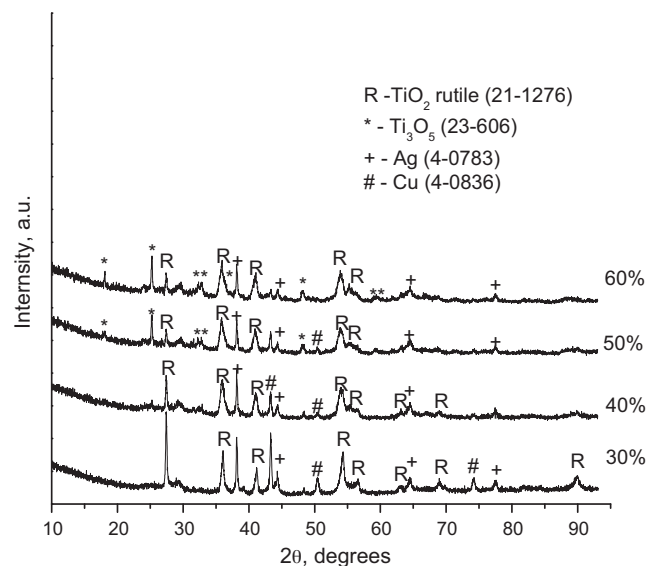


Fig. 3. XRD patterns of the detonation sprayed coatings (JCPDS card numbers of the identified phases are given in parentheses).

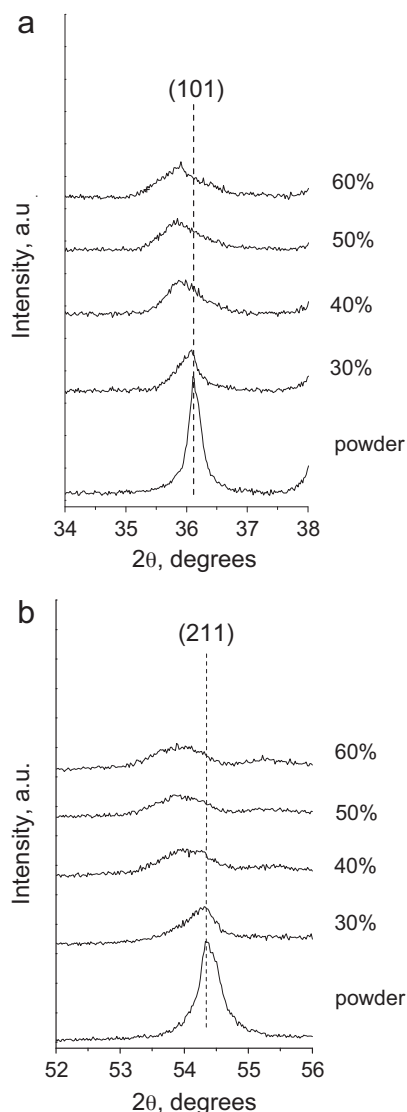


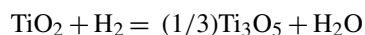
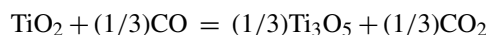
Fig. 4. Excerpts from the XRD patterns of the detonation sprayed coatings and milled  $\text{TiO}_2$ –2.5 vol.% Ag powder showing a shift of the (1 0 1) and (2 1 1) rutile peaks in the patterns of the coatings deposited high-temperature conditions.

The phase composition of the coating sprayed using an explosive charge of 30% does not show any significant differences from that of the sprayed powder (Fig. 3). Due to a limited thickness of the coatings, some XRD patterns contain diffraction lines of copper from the substrate. The mass of the material deposited per 1 shot of the gun was 2.0, 5.0, 8.0 and 8.8 mg for explosive charges of 30, 40, 50 and 60%, respectively, which shows an increased efficiency of spraying with increasing explosive charge.

In the XRD pattern of the coating deposited at an explosive charge of 40%, the intensity of the main reflection of rutile (1 1 0) decreases compared to that in the pattern of the coating produced at an explosive charge of 30%. The (1 0 1) and (2 1 1) reflections broaden and shift to lower angles, as can be seen from an enlarged view in Fig. 4. The (1 0 1) and (2 1 1) rutile reflections also shift to lower angles in the patterns of the coatings sprayed at an explosive charge of 50 and 60%.

Similarly, a shift of rutile reflections in the direction of lower angles has been observed in the patterns of suspension plasma-sprayed  $\text{TiO}_2$  coatings.<sup>21</sup> The reason of such changes is the formation of oxygen-deficient rutile in the reducing conditions. Indeed, as was calculated by Koudriachova,<sup>29</sup> lattice parameter  $a$  of the oxygen-deficient rutile increases up to 3% corresponding to the maximum possible concentration of oxygen vacancies in  $\text{TiO}_{1.9375}$ . Lattice parameter calculations from the peak positions on the corresponding XRD patterns show that in the coating deposited at an explosive charge of 60%, lattice parameter  $a$  of rutile increases 0.8% relative to that of the rutile phase in the milled powder.

In the coatings deposited at an explosive charge of 50 and 60%, titanium suboxide,  $\text{Ti}_3\text{O}_5$ , appears as a product of  $\text{TiO}_2$  reduction according to the following reactions:



The analysis of the observed changes in the intensities of rutile peaks in the patterns of the coatings did not allow us, however, to detect any preferred orientation of rutile, which was reported by Li and Ding<sup>30</sup> in the plasma sprayed  $\text{TiO}_2$ . This may be due to the complexity of the processes occurring in the detonation spraying under reducing conditions: melting, solidification and reduction reactions – all influencing the crystalline structure of  $\text{TiO}_2$ . A peculiar feature of the coatings sprayed in high-temperature reducing conditions is the presence of significant amounts of the  $\text{Ti}_3\text{O}_5$  phase, as is concluded from the XRD data. The analysis of the peak positions of the  $\text{Ti}_3\text{O}_5$  phase shows that the observed phase is the monoclinic  $\lambda$ -phase previously described in the literature.<sup>31–34</sup> At room temperature,  $\lambda$ - $\text{Ti}_3\text{O}_5$  is metastable and can be stabilized by doping.<sup>33</sup> In the detonation sprayed coating, this phase can form as a result of rapid cooling. Owing to its most interesting properties – metal-like conductivity and ability to undergo a room-temperature photo-reversible metal-semiconductor phase transition<sup>34</sup> –  $\lambda$ - $\text{Ti}_3\text{O}_5$  phase can be the target phase that modifies the electrical properties of the  $\text{TiO}_2$ -based coatings. Therefore, it is important to control its content in the deposited layers by varying the spraying parameters.

Particles, in which the melting temperature of rutile was not reached, form coatings with a porous structure (Fig. 5a and b). The coatings become denser and thicker as the explosive charge increases (Fig. 5c–h). The growing thickness of the coatings agrees well with an increased mass gain in the samples after the deposition. The coatings obtained with semi-molten and fully molten particles possess a lamellar structure typical for detonation sprayed coatings as is seen from the cross-sectional view of the coatings. In the coatings formed by molten particles, some flattened areas on the surface were observed (Fig. 6), which are direct indications of melting and solidification processes occurring in the sprayed material. Flattened areas were not found in the coating sprayed at an explosive charge of 30%, but occasionally detected at an explosive charge of 40%. In higher-temperature conditions realized at an explosive charge of 50%, flattened areas covered up to about a half of the

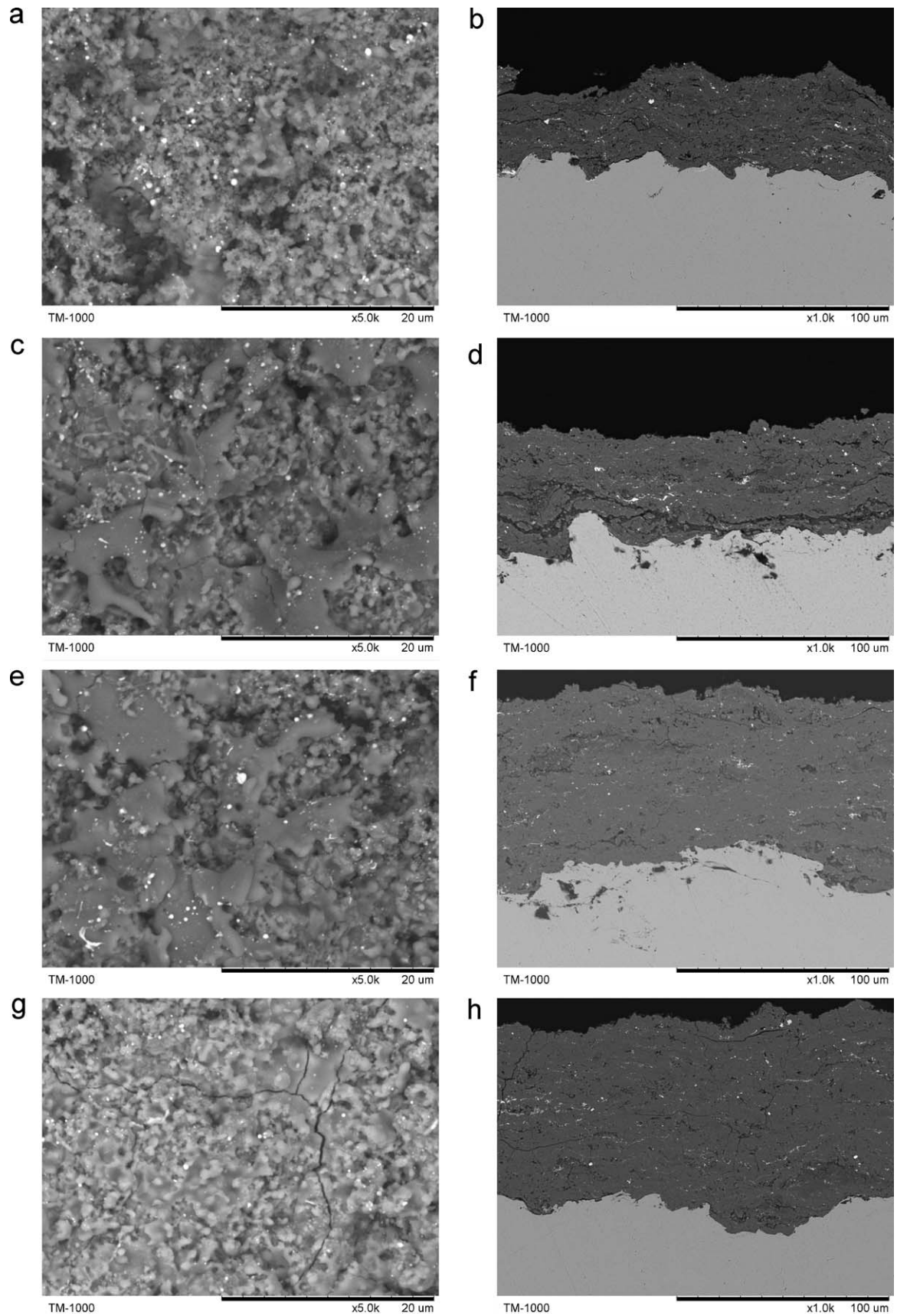


Fig. 5. SEM images of the surface and cross-sections of the detonation sprayed coatings obtained with different explosive charges: (a, b) 30%; (c, d) 40%; (e, f) 50%; (g, h) 60%.

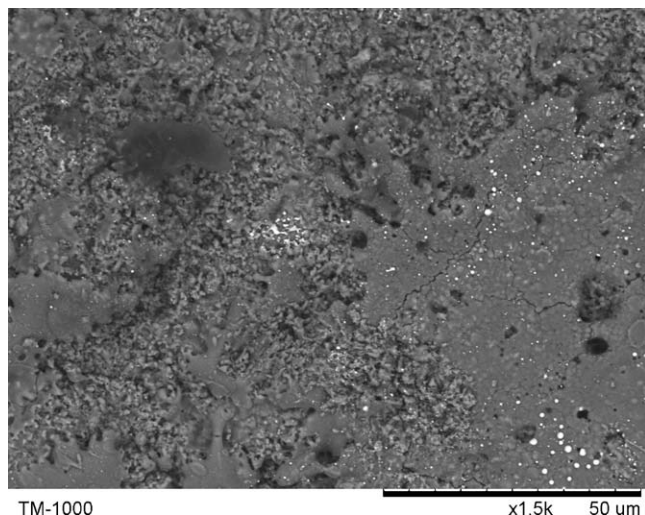


Fig. 6. SEM image of the surface the detonation sprayed coating showing flattened areas (explosive charge 50%).

coating surface. Interestingly, such flattened areas were only rarely found in the coatings formed at an explosive charge of 60%. Li et al.<sup>17</sup> observed a disappearance of frozen splats on the surface of the HVOF-sprayed  $\text{TiO}_2$  with increasing propane fuel flow and explained it by higher velocities of the sprayed particles and higher kinetic energies forcing particles to disperse upon impact with the substrate or previously deposited layers. In our case, particles sprayed at an explosive charge of 60% move more slowly than those at 50%. We believe that the particle temperature and the degree of overheating of the melt are as important since they influence the viscosity of the molten droplets. A droplet of a lower-viscosity melt is more likely to disperse upon impact with the substrate.

Bright particles that are easily distinguished in the back-scattered electron images of the surfaces and cross-sections of the coatings correspond to the silver inclusions as was confirmed by the EDS analysis. On the surface of the coatings, silver particles are in a frozen droplet shape. Though silver particles were molten in all conditions of spraying studied in this work, they were well preserved in the coatings and dispersed into fine droplets, which upon solidification formed submicron and nanoparticles. The silver inclusions located in the volume of the coating can be accessed through remaining pores and act as an antibacterial component.

#### 4. Conclusions

Thanks to the possibilities of varying the amount of an explosive gaseous mixture in Computer-Controlled Detonation Spraying, the particle temperatures and velocities as well as phase composition and microstructure can be controlled in a flexible manner. Detonation spraying of composite  $\text{TiO}_2$ –2.5 vol.% Ag powders was performed in a reducing atmosphere varying the amount of the explosive mixture  $\text{C}_2\text{H}_2 + 1.05\text{O}_2$ . In a cold mode of spraying, when the melting temperature of  $\text{TiO}_2$  was not reached, the coating had the phase composition of the feedstock powder. As larger volumes of the  $\text{C}_2\text{H}_2 + 1.05\text{O}_2$  mixture were

used, the particle temperature increased and  $\text{TiO}_2$  was reduced to form oxygen-deficient rutile and  $\lambda\text{-Ti}_3\text{O}_5$ . Silver inclusions in the titanium oxide matrix were preserved after high-temperature spraying and formed spherical particles in the coatings. This research has demonstrated that chemical reactions of reduction can be used as a tool of tailoring phase composition of the detonation sprayed oxide coatings.

#### Acknowledgements

The work was supported according to the Program of the Siberian Branch of Russian Academy of Sciences V.36.4. “Controlling chemical processes using high-pressures, radiation, and electrical and magnetic fields in stationary and impulse modes”, Integration Project Nos. 57 and 82 of the Siberian Branch of the Russian Academy of Sciences and Scientific School No. 5770.2010.1.

#### References

- Nikolaev YA, Vasiliev AA, Ulianitsky VY. Gas detonation and its application in engineering and technologies (review). *Comb Expl Shock Waves* 2003;**39**:382–410.
- Sova A, Pervushin D, Smurov I. Development of multimaterial coatings by cold spray and gas detonation spraying. *Surf Coat Technol* 2010;**205**:1108–14.
- Fauchais P, Montavon G, Bertrand G. From powders to thermally sprayed coatings. *J Therm Spray Technol* 2010;**19**:56–80.
- Ulianitsky V, Shtertser V, Zlobin S, Smurov I. Computer-controlled detonation spraying: from process fundamentals toward advanced applications. *J Therm Spray Technol* 2011;**20**:791–801.
- Carp O, Huisman CL, Reller A. Photoinduced reactivity of titanium dioxide. *Prog Solid State Chem* 2004;**32**:33–177.
- Paz Y. Application of  $\text{TiO}_2$  photocatalysis for air treatment: Patents’ overview. *Appl Catal B: Environ* 2010;**99**:448–60.
- Liu X, Zhao X, Fu RKY, Ho JPY, Ding C, Chu PK. Plasma-treated nanostructured  $\text{TiO}_2$  surface supporting biomimetic growth of apatite. *Biomaterials* 2005;**26**:6143–50.
- Avvakumov EG, Molchanov VV, Buyanov RA, Boldyrev VV. Crystallographic shear and catalytic activity of titanium dioxide. *Dokl Akad Nauk* 1989;**306**:367–70.
- Martyanov IN, Uma S, Rodrigues S, Klabunde KJ. Structural defects cause  $\text{TiO}_2$ -based photocatalysts to be active in visible light. *Chem Commun* 2004;**21**:2476–7.
- Martyanov IN, Berger T, Diwald O, Rodrigues S, Klabunde KJ. Enhancement of  $\text{TiO}_2$  visible light photoactivity through accumulation of defects during reduction-oxidation treatment. *J Photochem Photobiol A: Chem* 2010;**212**:123–41.
- Cozzoli PD, Fanizza E, Comparelli R, Curri ML, Agostiano A. Role of metal nanoparticles in  $\text{TiO}_2/\text{Ag}$  nanocomposite-based microheterogeneous photocatalyst. *J Phys Chem B* 2004;**108**:9623–30.
- Necula BS, Fratila-Apachitei LE, Zaat SAJ, Apachitei I, Duszczynk J. In vitro antibacterial activity of porous  $\text{TiO}_2$ –Ag composite layers against methicillin-resistant *Staphylococcus aureus*. *Acta Biomater* 2009;**5**:3573–80.
- Li B, Liu X, Meng F, Chang J, Ding C. Preparation and antibacterial properties of plasma sprayed nano-titania/silver coatings. *Mater Chem Phys* 2009;**118**:99–104.
- Rai M, Yadav A, Gade A. Silver nanoparticles as a new generation of antimicrobials. *Biotechnol Adv* 2009;**27**:76–83.
- Yang GY, Li CJ, Han F, Ohmori A. Microstructure and photocatalytic performance of high velocity oxy-fuel sprayed  $\text{TiO}_2$  coatings. *Thin Solid Films* 2004;**466**:81–5.

16. Liu X, Zhao X, Ding C, Chu PK. Light-induced bioactive TiO<sub>2</sub> surface. *Appl Phys Lett* 2006;**88**, 013905-1-3.
17. Li CJ, Yang GJ, Wang YY, Li CX, Ye FX, Ohmori A. Phase formation during deposition of TiO<sub>2</sub> coatings through high velocity oxy-fuel spraying. *Mater Trans* 2006;**47**:1690–6.
18. Berger LM. Titanium oxides – new opportunities for an established coating material. In: *Proc Intl Thermal Spray Conf*. ASM International; 2004. p. 934–45.
19. Toma FL, Berger LM, Jacquet D, Wicky D, Villaluenga I, de Miguel YR, Lindelov JS. Comparative study on the photocatalytic behaviour of titanium oxide thermal sprayed coatings from powders and suspensions. *Surf Coat Technol* 2009;**203**:2150–6.
20. Colmenares-Angulo JR, Cannillo V, Lusvarghi L, Sola A, Sampath S. Role of process type and process conditions on the phase content and physical properties of thermal sprayed TiO<sub>2</sub> coatings. *J Mater Sci* 2009;**44**: 2276–87.
21. Jaworski R, Pawlowski L, Pierlot C, Roudet F, Kozerski S, Petit F. Suspension plasma sprayed titanium oxide and hydroxyapatite coatings. In: *Proc Intl Thermal Spray Conf*. ASM International; 2009. p. 156–61.
22. Avvakumov EG, editor. *Fundamental bases of mechanical activation, mechanosynthesis and mechanochemical technologies*. Novosibirsk, Publishing House of the Russian Academy of Sciences; 2009 (in Russian).
23. Gavrilenko TP, Nikolaev YA, Ulianitsky VY, Kim MC, Hong JW. Computational code for detonation spraying process. In: *Proc intl thermal spray conf*. ASM International; 1998. p. 1475–83.
24. Smurov I, Pervushin D, Chivel Y, Laget B, Ulianitsky V, Zlobin S. Measurements of particle parameters at detonation spraying. In: *Proc intl thermal spray conf*. 2010. p. 481–95.
25. Zlobin SB, Ulianitsky VY, Shtertser AA, Smurov I. High-velocity collision of hot particles with solid substrate under detonation spraying: detonation splats. In: *Proc intl thermal spray conf*. 2009. p. 728–34.
26. Li Y, Ishigaki T. Thermodynamic analysis of nucleation of anatase and rutile from TiO<sub>2</sub> melt. *J Cryst Growth* 2002;**242**:511–6.
27. E.A.Brandes, G.B.Brook (Eds.), *Smithells metal reference handbook*, 7th ed., Butterworth-Heinemann, 1998.
28. Glushko VP. Thermodynamic properties of individual compounds, v.4, book 2, Moscow, Nauka, USSR, 1982.(in Russian).
29. Koudriachova M. Geometry and ordering of defects in non-stoichiometric rutile. *Phys Stat Sol* 2007;**4**:1205–8.
30. Li JF, Ding CX. Crystalline orientation of plasma-sprayed TiO<sub>2</sub> coatings. *J Mater Sci Lett* 1998;**17**:1747–9.
31. Onoda M, Ogawa Y, Taki K. Phase transitions and the doping effect in Ti<sub>3</sub>O<sub>5</sub>. *J Phys: Condens Matter* 1998;**10**:7003–13.
32. Gusev AA, Avvakumov EG, Medvedev AZ, Masliy AI. Ceramic electrodes based on magneli phases of titanium oxides. *Sci Sin* 2007;**39**:51–7.
33. Grass V, Istomin P, Nazarova L. X-ray diffraction refinement of the crystal structure of anosovite prepared from leucoxene. *Cryst Res Technol* 2009;**44**:117–22.
34. Ohkoshi S, Tsunobuchi Y, Matsuda T, Hashimoto K, Namai A, Hakoe F, Tokoro H. Synthesis of a metal oxide with a room-temperature photoreversible phase transition. *Nature Chem* 2010;**2**:539–45.